# Optimum Me-DLC Coatings and Hard Coatings for Tribological Performance

*Y.L. Su and W.H. Kao*

*(Submitted 29 December 1998; in revised form 18 October 1999)*

**In this study, hard coatings (TiN, TiCN, CrN, and CrCN) and Me-DLC coatings ($Ti_{x\%}$-C:H and $Cr_{x\%}$-C:H) were deposited on tungsten carbide (WC) substrate by multiarc physical vapor deposition (MAPVD) and unbalanced magnetron (UBM) sputtering, respectively. Counterbodies of the AISI 1045 steel cylinder and the AA7075T651 aluminum cylinder were used in the cylinder-on-disk, line-contact wear mode under dry condition; a counterbody of the AISI 52100 steel ball was used in the ball-on-disk, point-contact wear mode, under both dry and lubricated conditions. All wear tests were conducted with a reciprocating machine. After the tests, the most suitable coating for various counterbodies and test environments was selected. For the coating/1045 steel cylinder, the $Ti_{10\%}$-C:H coating possesses excellent tribological characteristics. For the coating/7075T651 aluminum cylinder, hard coatings display excellent wear resistance. For the coating/steel ball, CrCN and CrN coatings display very little wear under both dry and lubricated conditions. On TiN and TiCN coatings, special wear mechanisms of material transfer, adhesion wear, and fatigue fracture occurred during initial tests under kerosene lubrication.**

**Keywords** hard coating, Me-DLC, tribology

## 1. Introduction

Applying a thin hard coating to the sliding surfaces of machine parts reduces wear and extends the service life of the parts. Coatings such as titanium nitride (TIN), titanium carbide (TiC),[1–5] and titanium carbonitride (TiCN),[6,7,8] are widely used in industrial applications. In addition, chromium nitride (CrN)[9–12] and chromium carbonitride (CrCN)[13] coatings have been researched to assess their wear resistance characteristics. Hard coatings reduce wear rates of parts and tools. However, when dealing with sliding wear pairs of hard coatings/counterbody, problems arise. These problems include high friction coefficients, seizure behavior, loud noise, and severely damaged counterbody. Other coatings, with low friction coefficients and lower hardness, such as PbO, $MoS_2$, and graphite, have been deposited as solid lubricants. Although such coatings have low friction coefficients, their relative softness results in more wear. Recent research proves that using diamond-like carbon (DLC) or amorphous hydrogenated carbon (*a*-C:H) films can reduce friction coefficients and the wear rate without applying liquid lubricants on a sliding interface.[14–18] These characteristics have been successfully used as a low-load protective coating for both magnetic and optical disks.[19,20] However, the high levels of internal stress in DLC coatings and their poor adhesion near the coating/substrate interface have limited their use in engineering applications.

The adhesion of the DLC coating can be improved using a graded transition from TiN-TiCN to amorphous hydrogenated carbon[21] or a multiple stack of metal/DLC and carbide/DLC nanolayers.[22] To reduce the internal stress of the DLC coating, some studies have advocated the metal doping of the DLC layer.[23–27] Recent research has presented a gradient design using a gradual metal/ceramic/DLC transition that improved load support and adhesion strength.[28,29,30]

In light of the above development, we deposited Me-DLC coatings Ti doping and Cr doping ($Ti_{x\%}$-C:H and $Cr_{x\%}$-C:H) on tungsten carbide (WC) substrates, using unbalanced magnetron (UBM) sputtering. We also deposited hard coatings of TiN, TiCN, CrN, and CrCN on WC substrates using multiarc physical vapor deposition (MAPVD). The tribological behavior of Me-DLC coatings, $Ti_{x\%}$-C:H and $Cr_{x\%}$-C:H, and hard coatings, TiN, TiCN, CrN, and CrCN, were compared to find suitable coatings for different sliding wear pairs.

**Y.L. Su** and **W.H. Kao**, Department of Mechanical Engineering, National Cheng Kung University, Tainan, Taiwan. Contact e-mail: n1885115 @ sparc1.cc.ncku.edu.tw.

**Table 1 The chemical compositions of specimens (wt.%)**

| Composition | Fe | C | Si | Mn | P | S | Ni | Cu | Cr |
|---|---|---|---|---|---|---|---|---|---|
| AISI 1045 | Bal. | 0.46 | 0.24 | 0.75 | 0.02 | 0.01 | 0.06 | 0.05 | 0.21 |
| AISI 52100 | Bal. | 1.03 | 0.22 | 0.31 | 0.01 | 0.01 | 0.07 | 0.06 | 1.39 |
| Composition | Al | Fe | Si | Mn | Ti | Mg | Zn | Cu | Cr |
| AA 7075T651 | Bal. | 0.5 | 0.4 | 0.3 | 0.2 | 2.5 | 5.6 | 1.6 | 0.23 |

## 2. Experimental Details

### 2.1 Specimen Preparation

The study used AISI 1045 steel (cylinder), AA 7075T651 aluminum (cylinder), and AISI 52100 (ball) steel materials as upper specimens for Schwingung Reibungund Verschleiss (SRV) tests, whereas the material of the lower specimen was WC (bulk disk). Table 1 lists the chemical compositions of the 1045 steel, the 7075T651 aluminum, and the 52100 steel. The WC bulk disk is a powder metallurgy sintered part containing 6wt.%Co. The average size of the WC particles was ~0.5 μm. The fully mixed powders of WC and Co were compressed to a density of 14.73 g $cm^{-3}$, followed by presintering at 600 to 1000 °C for 30 min; the powders were then sintered in a vacuum for 2 to 3 h at 1450 to 1500 °C.[31] After this process, the WC specimen was mechanically polished to a roughness of Ra = 0.008 μm, ultrasonically cleaned in acetone, and kept in an electric dryer to prevent its contamination.

### 2.2 Lubricants

The lubricants used in this study included a tradename of HD-150 and kerosene (Chinese Petroleum Co. (Taipei, Taiwan)). The HD-150 possesses a kinematic viscosity of 138.9 cSt at 40 °C and 14.4 cSt at 100 °C, which contains sulfur and chlorine that form a sustainability of high pressure. The kerosene is ordinarily used to wash greasy machine parts or as the fuel for kerosene lamps or for airplanes.

### 2.3 Deposition of Coatings

***Me-DLC Coatings.*** $Ti_{x\%}$-C:H and $Cr_{x\%}$-C:H films were deposited on WC bulk disks based on a technique using the UBM sputtering (UDP-450, Teer Coatings, Worcestershire, UK) process and the closed-loop optical emission monitoring (OEM) control system. Sputtering was performed in an Ar atmosphere and $N_2$ and $C_2H_2$ were used as reaction gases. For instance, the process of $Ti_{x\%}$-C:H coating deposition is as follows.

First, a layer of Ti of about 0.1 μm thickness is deposited on each specimen. After deposition of the Ti layer, nitrogen is introduced to produce a layer of TiN. Then, $C_2H_2$ is introduced gradually to produce a TiCN layer. After that, the provision of the nitrogen is gradually turned off and at the same time the flow of $C_2H_2$ is increased to produce a TiC layer. Finally, the $C_2H_2$ flow is further increased gradually to cause more poisoning of the Ti target. An optical emission spectrometer is used to measure the intensity of Ti emission from one of the targets. The $C_2H_2$ flow is then admitted through a piezoelectric valve until the intensity of the emission line has dropped to a preselected value. The spectrometer and the piezoelectric valve are then switched into a closed-loop system to stabilize partial pressure of the reactive gas at this level. As a result, the Ti metal and hydrocarbon are sputtered simultaneously from the poisoned target surface to produce a $Ti_{x\%}$-C:H layer. The OEM control allows the deposition of films with the required metal composition formed by monitoring the ratio, *x*%, of target "poisoning" in the relative intensity of the selected titanium emission line reference to the intensity from a nonpoisoned target. The final composition of the $Ti_{x\%}$-C:H coating will depend on the degree of this target poisoning by the hydrocarbon. The $Cr_{x\%}$-C:H coating was deposited in a similar process. Table 2 displays the parameters of deposition, and Fig. 1 indicates the structure of the coatings.

***Hard Coatings Deposition.*** Hard coatings of TiN, TiCN, CrN, and CrCN were deposited on WC bulk disks by using the HC-1000 MAPVD system (Hauzer Techno Coating, Venlo, Holland). The deposition parameters are listed in Table 3.

To enhance adhesion of the coating, an interface layer of about 0.1 μm thickness (Ti for TiN and TiCN or Cr for CrN and CrCN) was deposited between the WC substrate and the coating. The deposition procedure for TiN, for instance, was described as the following. (1) The target was heated to evaporation temperature and pure Ti was then evaporated and deposited onto the specimens. (2) Nitrogen gas was subsequently introduced into the deposition chamber, and TiN then began to grow on the pure Ti layer. The film thickness was controlled

**Table 2 The deposition parameters for $Ti_{x\%}$-C:H and $Cr_{x\%}$-C:H coatings**

| Parameters | $Ti_{x\%}$-C:H and $Cr_{x\%}$-C:H coating |
|---|---|
| Reaction gases | $N_2$ and $C_2H_2$ |
| Chamber pressure (mbar) | $1 \times 10^{-2}$ |
| Bias voltage (V) | –50 |
| Arc current (A) | 6 |
| Chamber temperature (°C) | 150 |
| Evaporation temperature (°C) | 150 |
| Evaporation rate (μm/h) | 2 |

**Table 3 Deposition parameters for TiN, TiCN, CrN, and CrCN**

| | Films | | | |
|---|---|---|---|---|
| Parameters | TiN | TiCN | CrN | CrCN |
| Partial pressure of $N_2$ (mbar) | $1 \times 10^{-2}$ | $4 \times 10^{-3}$ | $4 \times 10^{-3}$ | $4 \times 10^{-3}$ |
| Partial pressure of $CH_4$ (mbar) | . . . | $6 \times 10^{-3}$ | . . . | . . . |
| Partial pressure of $C_2H_6$ (mbar) | . . . | . . . | . . . | $6 \times 10^{-3}$ |
| Chamber pressure (mbar) | $1 \times 10^{-2}$ | $1 - 10^{-2}$ | $1 - 10^{-2}$ | $1 \times 10^{-2}$ |
| Bias voltage (V) | –120 | –120 | –120 | –120 |
| Arc current (A) | 80 | 80 | 80 | 80 |
| Chamber temperature (°C) | 400 | 400 | 400 | 400 |
| Evaporation temperature (°C) | 400 | 400 | 400 | 400 |
| Evaporation rate (μm/h) | 4 | 4 | 3.2 | 2.2 |

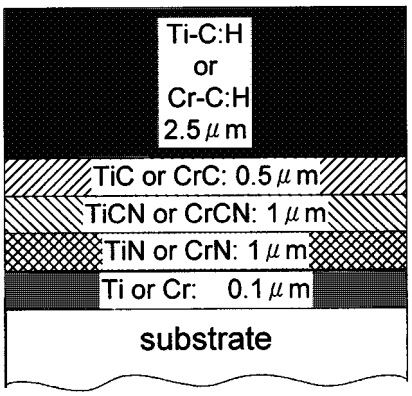


**Fig. 1** Schematic diagram of the gradual Ti/TiN/TiCN/TiC or Cr/CrN/CrCN/CrC medilayer from substrate to $Ti_{x\%}$-C:H or $Cr_{x\%}$-C:H topcoat

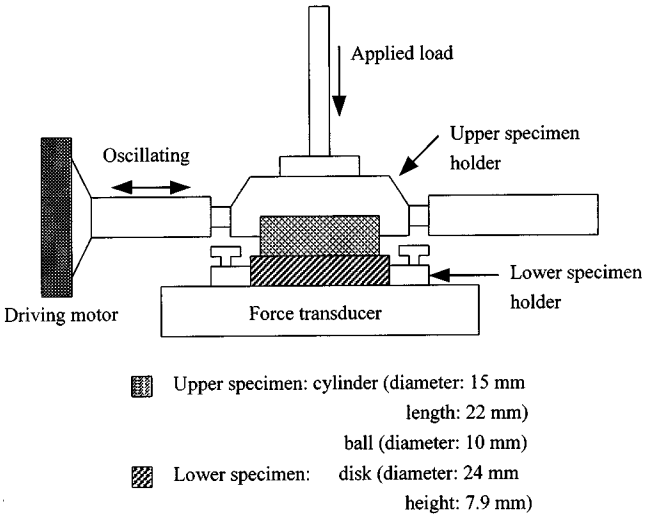


**Fig. 2** SRV wear test machine

by adjusting the depositing time. The CrN coating was obtained in a similar process. Formation of TiCN was achieved by introducing $CH_4$ into the TiN-depositing chamber, and the pressure ratio of $N_2$:$CH_4$ was controlled at 2:3. In this study, the constitution of TiCN was 0.1 μm of Ti plus 2.5 μm of TiN plus 2.5 μm of TiCN, started from the substrate to the outmost layer. The CrCN coating was obtained in a similar process and was composed of 0.1 μm of Cr plus 2.5 μm of CrN plus 2.5 μm of CrCN.

### 2.4 Mechanical Properties Test

The hardness of the coating films was measured with a nanoindentation tester (Fischerscope H100B, Fischer Technology Inc., Sindefinger, Germany). To measure the mechanical properties of the coating films, the penetration depth of the indenter should be limited to 10% of the film thickness (all of the penetration depths in this study were below 0.5 μm). In addition, the force at initial contact was 0.4 mN, time between two load steps was 1 s, total time for loading was 39 s, and force at final contact was 100 mN. Notably, the measured values were the outcome of the mixed property of the topcoat and medilayer.

### 2.5 Wear Test

Wear tests were performed by using an SRV reciprocating sliding machine (Optimal, München, Germany). The SRV test machine consists of a fixed lower specimen supporter and a replaceable upper specimen holder. The upper specimen can be a ball or a cylinder block, depending on what type of holder is being used, and the lower specimen is a disk. Figure 2 displays the dimensions of the test specimens and a schematic diagram of the experimental setup.

The arrangement of a ball or a cylinder block mated with a disk formed a ball-on-disk, point-contact wear mode or a cylinder-on-disk, line-contact wear mode, respectively. The tests were performed at room temperature and atmospheric pressure. The relative humidity of the laboratory was about 45 to 55%. In addition, a constant 1 mm stroke, 100 N normal load, 24 min test duration (144 m slide distance), and 50 Hz frequency were employed. The maximum depth of wear scars on a lower test contacted disk were taken by using a surface profilometer (Kosake SE30H Kosaka Laboratory Ltd., Tokyo, Japan) with a precision of ±0.005 μm at a magnification of $\times 10^6$.

All of the tests were performed twice and three different measurements were taken from each pass of the tests. Then, the six measurements from the same tests were averaged and are shown as the measurement results in this work.

## 3. Results

### 3.1 Hardness, Composition, and Adhesion

Table 4 lists the microhardness values of Me-DLC coatings ($Ti_{x\%}$-C:H and $Cr_{x\%}$-C:H) and hard coatings (TiN, TiCN, CrN, and CrCN). The microhardness values were found to increase with increasing metal content (increasing $x$% level) of $Ti_{x\%}$-C:H and $Cr_{x\%}$-C:H coatings, as demonstrated in Table 4. The Me-DLC coatings also have lower microhardnesses than the TiN, TiCN, CrN, and CrCN coatings. CrCN (4430 kg/mm$^2$) and $Ti_{10\%}$-C:H (930 kg/mm$^2$) have the highest and lowest microhardnesses, respectively. The $Ti_{x\%}$-C:H and $Cr_{x\%}$-C:H coatings had varying ratios of target poisoning, as analyzed by a wavelength dispersive spectrometer (WDS). $Ti_{x\%}$-C:H coatings with $x$ = 10 and 20% poisoning levels contain approximately 90 and 82% of carbon atoms, respectively. However, at the $x$ = 30% poisoning level, the percentage of carbon atoms markedly decreases to 59%. On the other hand, the $Cr_{x\%}$-C:H coatings contain approximately 75, 60, and 43% of carbon atoms, corresponding to poisoning levels of $x$ = 10, 20, and 30%, respectively. Table 5 shows the element composition of $Ti_{x\%}$-C:H and $Cr_{x\%}$-C:H coatings.

A scratch tester was used to drive a 300 μm diameter diamond stylus across the coatings to determine the coating adhesion at a continuously increased loading rate of 1 N s$^{-1}$. The nominal maximum load was 70 N. Scratch tests indicated the following three scratch failures with different coatings. (1) $Ti_{30\%}$-C:H coating started with conformal cracking inside the track and wedged

**Table 4 Total thickness, hardness, and wear results of the coating disk under various conditions specified in this experiment (wear on disk is measured in depth; the unit for wear is μm)**

| | | | Cylinder on disk | | 52100 steel ball on disk | | |
|---|---|---|---|---|---|---|---|
| Coating | Total thickness (μm) | Hardness (kg/mm²) | 1045 steel dry | 7075 Al dry | Kerosene dry | | HD-150 |
| $Ti_{10\%}$-C:H | 5.1 | 930 | 1.5 | 5.1 | 7.0 | 2.5 | 2.4 |
| $Ti_{20\%}$-C:H | 5.1 | 1,399 | 2.2 | 4.5 | 6.5 | 3.9 | 3.3 |
| $Ti_{30\%}$-C:H | 5.1 | 2,743 | 5.4 | 4.0 | 6.8 | 4.2 | 4.2 |
| TiN | 5.1 | 2,760 | 2.7 | 1.0 | 1.5 | 5.0 | 0.3 |
| TiCN | 5.1 | 2,850 | 2.5 | 1.5 | 1.4 | 5.0 | 0.2 |
| $Cr_{10\%}$-C:H | 5.1 | 1,173 | 1.9 | 3.5 | 5.8 | 2.3 | 1.6 |
| $Cr_{20\%}$-C:H | 5.1 | 1,738 | 1.8 | 2.6 | 5.3 | 1.4 | 1.2 |
| $Cr_{30\%}$-C:H | 5.1 | 2,707 | 1.5 | 2.2 | 5.1 | 0.6 | 0.7 |
| CrN | 5.1 | 3,300 | 1.5 | 1.4 | 1.1 | 0.4 | 0.2 |
| CrCN | 5.1 | 4,430 | 1.5 | 1.2 | 1.1 | 0.2 | 0.2 |

**Table 5 WDS analysis of element composition of $Ti_{x\%}$-C:H and $Cr_{x\%}$-C:H coatings with different ratios of Ti or Cr target poisoning**

| | Elements composition (at.%) | | | | |
|---|---|---|---|---|---|
| Coatings | C | Ti | Cr | N | O |
| $Ti_{10\%}$-C:H | 90.2 | 3.5 | . . . | 2.8 | 3.5 |
| $Ti_{20\%}$-C:H | 82.6 | 7.7 | . . . | 3.2 | 6.5 |
| $Ti_{30\%}$-C:H | 58.9 | 34.4 | . . . | 4.1 | 2.6 |
| $Cr_{10\%}$-C:H | 75.2 | . . . | 19.0 | 3.8 | 5.0 |
| $Cr_{20\%}$-C:H | 60.5 | . . . | 27.3 | 4.2 | 3.8 |
| $Cr_{30\%}$-C:H | 43.3 | . . . | 45.5 | 3.2 | 1.8 |

cracking beside the track, followed by adhesive failure with gross spallation, which led to exposure of the WC substrate, as shown in Fig. 3(a) and (b). This implies a relatively poor adhesion. The critical point is defined as the point where the substrate was revealed in the scratch track (indicated by the arrow in Fig. 3a). The critical load is about 56 N. (2) TiCN coating displays the symmetrical shelllike chipping that appeared at both sides of the scratch track, as shown in Fig. 3(c). The maximum depth of measured shelllike chipping regions is 2.5 μm (total thickness of TiN + TiCN is 5 μm); therefore, Fig. 3(c) shows a cohesive failure of the TiN/TiCN interface. The initial shelllike chipping took place under a load of about 63 N (indicated by the arrow in Fig. 3c). (3) Other coatings do not reveal any cracking, flaking, or tearing on the scratch track or ridges of the coatings. This could be attributed to a good adherence.

### 3.2 Tribological Behavior

This study evaluated the tribological performance of these coatings under dry and lubricated (HD-150 and kerosene) environments; friction coefficients were also recorded continuously during the tests. In dry sliding tests, each coating was tested with a cylinder-on-disk, line-contact arrangement, under a set of fixed parameters. These coatings were also tested with a ball-on-disk, point-contact arrangement, under dry and lubricated conditions. Table 4 lists the maximum depth of wear scars on all coating disks tested under dry and lubricated conditions using HD-150 and kerosene. These experiments investigated the tribological behavior and the suitability of coatings for wear resistance under various conditions.

***Line Contact Wear Mode.*** A cylinder-on-disk, line-contact wear mode was employed to investigate the wear behavior of the coating disks under dry conditions. Figure 4 displays the wear results of these coatings against 1045 steel cylinder. The $Ti_{10\%}$-C:H coating is the most suitable coating used for wear resistance, even though it has the lowest microhardness (Table 4). Intriguingly, even though $Ti_{10\%}$-C:H and $Ti_{20\%}$-C:H are inferior to the hard coatings of TiN and TiCN in microhardness, they perform even better than the hard coatings against 1045 steel cylinder. On the other hand, even though the microhardness of coating $Ti_{30\%}$-C:H is almost equivalent to the microhardness of hard coatings TiN and TiCN, $Ti_{30\%}$-C:H displays very poor wear resistance. Figure 4 reveals the wear results for $Cr_{x\%}$-C:H, CrN, and CrCN coatings. These coatings display a better wear resistance than all other coatings except $Ti_{10\%}$-C:H. Figure 4 also displays the results of wear depth tests on coating disks sliding against the 7075T651 aluminum cylinder. All of the $Ti_{x\%}$-C:H coatings were worn through, almost to the substrate. The $Cr_{x\%}$-C:H coatings also displayed severe wearing, 1.5 to 2 times the wear depth of sliding against a 1045 steel cylinder. The coating/7075T651 Al contact surfaces severely damaged the disks with $Cr_{x\%}$-C:H and $Ti_{x\%}$-C:H coatings, as described in "Coatings Sliding against 7075T651 Al Cylinder." On the other hand, all hard coatings of TiN, TiCN, CrN, and CrCN displayed an excellent wear resistance sliding against 7075T651Al.

Figure 5 summarizes three typical curves of friction coefficients as follows: (1) The curves for $Ti_{x\%}$-C:H coatings with $x$ = 10 and 20% levels against the 1045 steel cylinder are low and smooth, owing to a transfer layer that provided a lubricating effect between the contact surfaces formed. (2) Other coatings ($Ti_{30\%}$-C:H, $Cr_{x\%}$-C:H with $x$ = 10, 20, and 30%, TiN, TiCN, CrN, and CrCN) present high and fluctuating curves because of the adhesive wear and oxidative wear that took place on the contact surfaces during wear tests. (3) All traces of friction coefficients for Me-DLC and hard coatings against the 7075T651 Al cylinder depict a large fluctuation and multiple seizures (indicated by the spikes on the curve), as shown in Fig. 6. The wear pairs of coating/7075T651 Al formed a transfer layer on the coating disk, and adhesion wear took place on the contact surfaces; this severely damaged the Me-DLC coat-

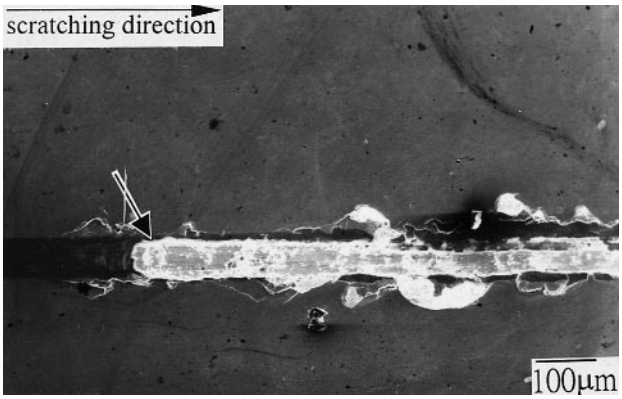


**(a)**

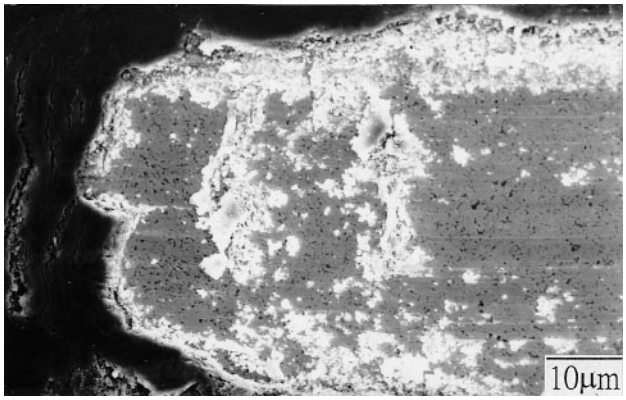


**(b)**

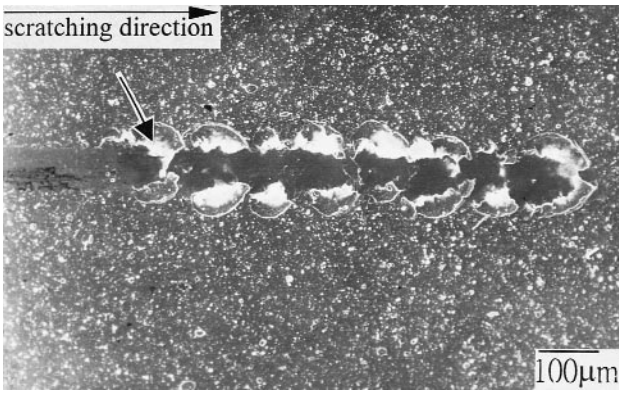


**(c)**

**Fig. 3** **(a)** Scratch results of the $Ti_{30\%}$-C:H coating. **(b)** Magnified micrograph of **(a)**. **(c)** Scratch result of the TiCN coating

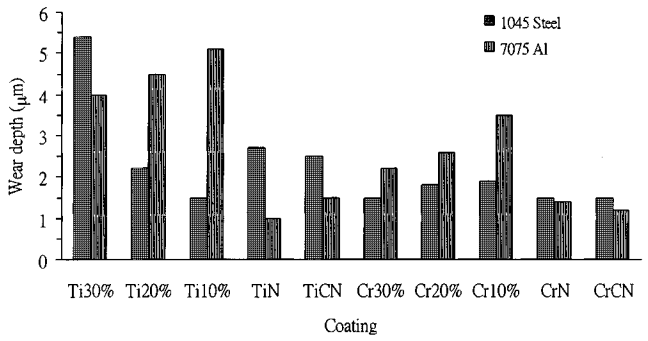


**Fig. 4** Wear depth of coating disks against the 1045 steel and 7075T651 aluminum cylinder, respectively, under dry condition (Ti30% stands for $Ti_{30\%}$-C:H, Cr30% stands for $Cr_{30\%}$-C:H, *etc.*)

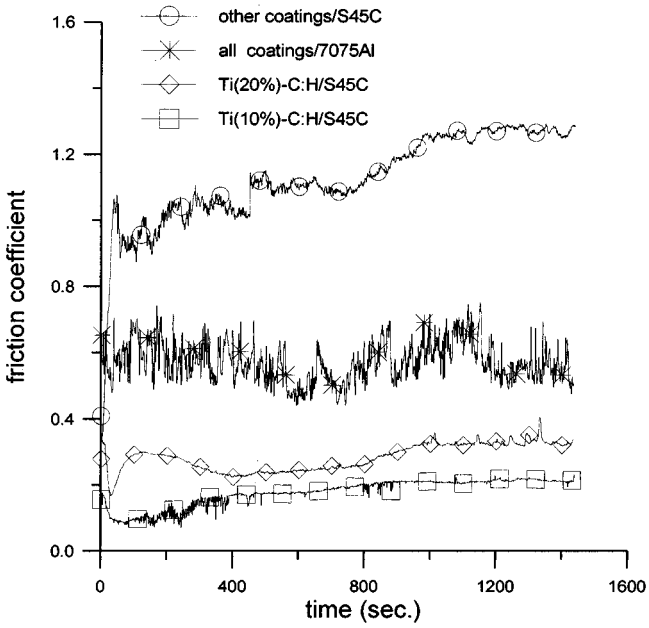


**Fig. 5** Typical traces of friction coefficients of various coatings in cylinder on disk with the 1045 steel cylinder and 7075T651 A1 cylinder under dry condition, respectively. For those against 1045 steel, only $Ti_{x\%}$-C:H with $x$ = 10 and 20% displayed a low value; other coatings ($Cr_{x\%}$C:H, $Ti_{30\%}$-C:H, and hard coatings) displayed a high value. For those against 7075T651 A1, all coatings displayed a large fluctuation and multiple seizures (spikes on the trace)

ing disks, as described in "Coatings Sliding against 7075T651 Al Cylinder."

***Point Contact Wear Mode.*** Tests using the ball-on-disk, point-contact wear mode assessed the wear behavior of the Me-DLC coatings and the hard coatings under dry and lubricated conditions. Figure 6 displays the results of. the wear tests. The $Ti_{x\%}$-C:H coatings reveal poor wear resistance against the steel ball, under either dry or lubricated condition. Coatings of TiN and TiCN, which have better wear resistance than $Ti_{x\%}$-C:H and $Cr_{x\%}$-C:H coatings under dry and HD-150 lubricated conditions, both display a very poor wear resistance under kerosene-lubricated condition. Coatings of TiN and TiCN even possess a deeper wear depth under kerosene-lubricated condition than under dry condition. The tribological behavior of a steel ball sliding against TiN and TiCN coatings under kerosene-lubricated condition displays a special wear mechanism. $Cr_{x\%}$-C:H coatings possess a better wear resistance than $Ti_{x\%}$-C:H coatings under lubricated conditions. Under dry conditions, however, $Cr_{x\%}$-C:H coatings become severely damaged, even wearing through to the substrate. On the other hand, both CrN and CrCN coatings reveal an excellent wear resistance under

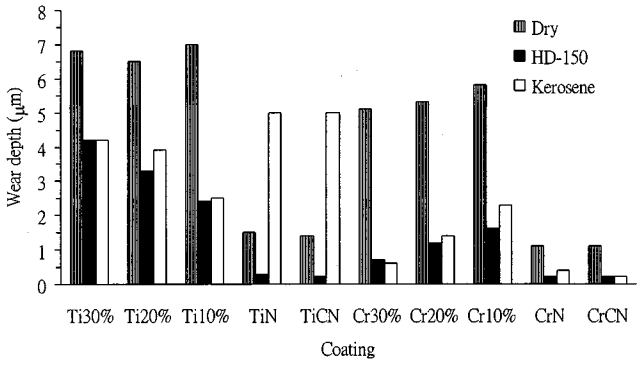


**Fig. 6** Wear depth of coating disks against steel ball under dry and lubricated conditions (Ti30% stand for $Ti_{30\%}$-C:H, Cr30% stands for $Cr_{30\%}$-C:H, *etc*.)

both dry and lubricated conditions; these coatings have good potential in wear resistance.

All the curves of friction coefficients, except for wear pairs of the TiN/steel ball and TiCN/steel ball, are low and smooth under the HD-150 or kerosene-lubricated conditions, as shown in Fig. 7(a). The wear pairs of the TiN/steel ball and TiCN/steel ball display an initial high friction coefficient (between 0.6 and 0.9) for about 31 s under kerosene lubrication, as shown in Fig. 7(b). This phenomenon indicates that, initially, a specific tribological behavior on the contact surfaces induced severe wear on disks coated with TiN and TiCN, as discussed in Section 4.3. Figure 8 summarizes two typical curves of the friction coefficients of coating/steel ball wear pairs, under dry condition. One is the $Ti_{10\%}$-C:H/steel ball wear pair, which reveals low friction coefficients (about 0.1) during the initial stage (about 87 s) and then suddenly increases up to 0.8, along with a fluctuation trace. The above demonstrates that the $Ti_{10\%}$-C:H coating, which has a higher carbon content, initially acts as a solid lubricant on the contact surfaces but wears out to the medilayer after the initial stage, under the high contact pressure and reciprocating motion between the contact surfaces. It thereby induces adhesive wear with high friction coefficients during the test. The other wear pairs all maintained a high and fluctuating curve of friction coefficients all through the wear tests. Adhesive wear or abrasive wear was the main wear mechanism.

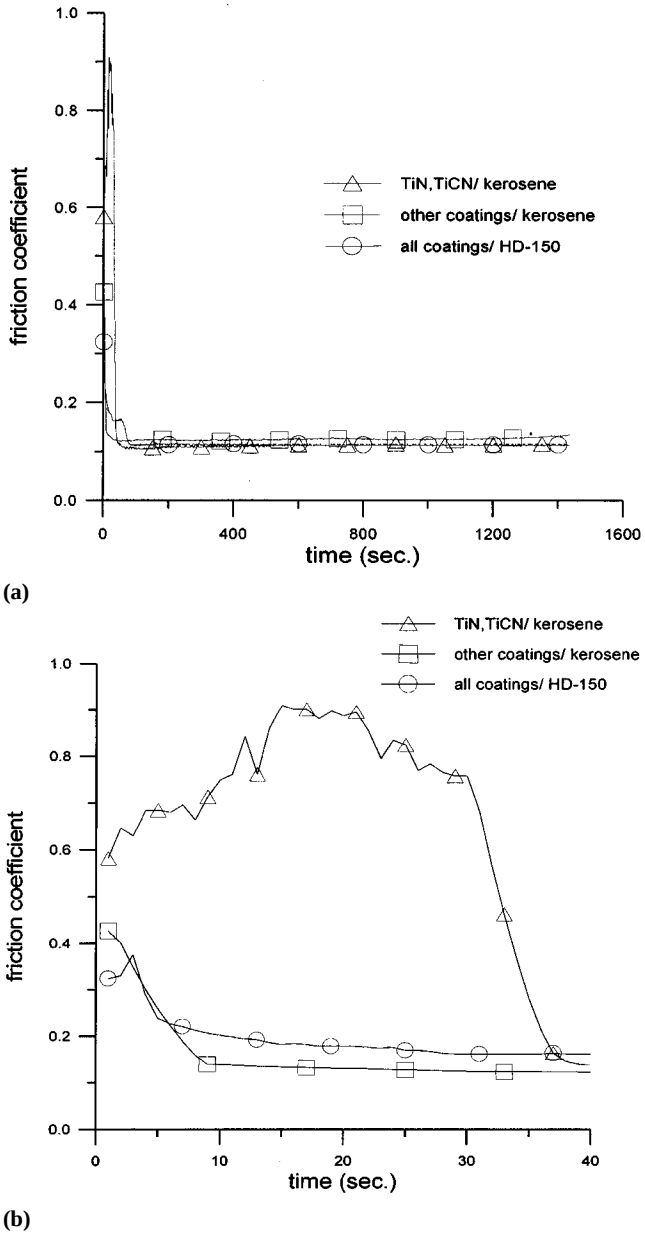


**Fig. 7** Typical traces of friction coefficients for the ball-on-disk, point-contact wear mode under lubricated conditions. **(a)** The TiN or TiCN coatings display an initial high friction coefficient, while the other coatings display low friction coefficients throughout the wear test under kerosene-lubricated condition. All coatings display low friction coefficients under HD-150 lubricated condition. **(b)** Initial traces of local friction coefficients of **(a)**

## 4. Discussion and Wear Mechanism

### 4.1 Dry Wear

***$Ti_{x\%}$-C:H Coatings Sliding against 1045 Steel.*** Wear behavior of the $Ti_{x\%}$-C:H coatings can be classified into two groups. Group 1:$Ti_{x\%}$-C:H coatings with $x$ = 10 and 20% levels sliding against 1045 steel under dry condition. The traces of the friction coefficients of these coatings were smooth and low with only very slight noise. Figures 9(a) and (b) display the typical worn surface of the coating disk and the energy dispersive spectrometer (EDS) analysis of Fig. 9(a), respectively. Figure 9(a) reveals that there are some mild grooves with micropits on the smooth worn surface. Figure 9(b) demonstrates that there is no Fe element transfer from the counterbody 1045 steel cylinder to the worn surface. A transfer layer was formed on the counterbody 1045 steel cylinder from the coating disk, as shown in Fig. 10(a). The original machining mark of the 1045 steel cylinder can be clearly observed below this transfer layer. For further analysis, the transfer layer on the 1045 steel cylinder was cleaned out after the wear test, as shown in Fig. 10(b). Figure 10(b) indicates that nearly zero wear occurred on the 1045 steel cylinder during the test. Obviously, the

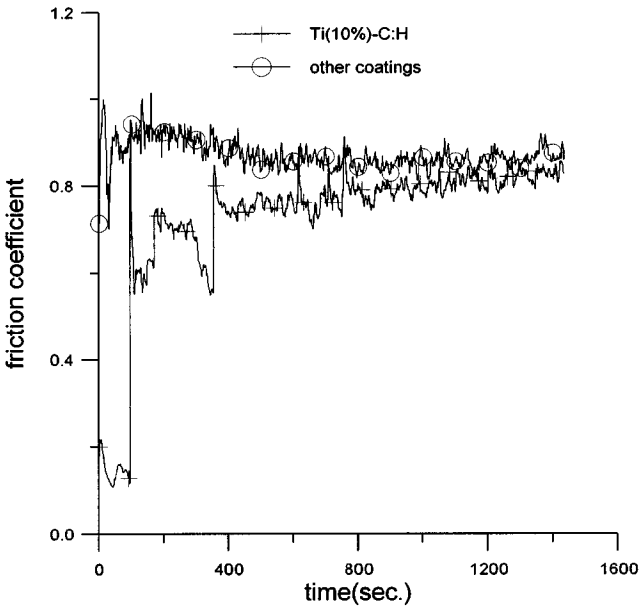


**Fig. 8** Two typical traces of friction coefficients of various coatings in the ball-on-disk, point-contact wear mode under dry condition. One of the $Ti_{10\%}$-C:H coatings possessed low friction coefficients at the beginning of the wear test (about 87 s); other coatings displayed high friction coefficients throughout the wear test

$Ti_{10\%}$-C:H and $Ti_{20\%}$-C:H coatings that contained more carbon-rich material supplied a solid lubricant effect to reduce friction. Additionally, a protective transfer layer was formed on the 1045 steel cylinder from the coating disk. In fact, friction behavior between the coating disk and the transferred layer of the 1045 steel cylinder accounts for a positive effect on the tribological behavior. Group 2: When $x$ = 30% in $Ti_{x\%}$-C:H coating sliding against 1045 steel under dry condition, its trace of friction coefficients presents a high value and a fluctuation. This finding suggests that adhesive wear occurs under dry condition. Furthermore, a short wear test confirmed that adhesion behavior took place between the contact surfaces of this wear pair. After testing for 50 s, the maximum wear depth was only 1 μm on the coating disk (the coating was not worn out because the $Ti_{30\%}$-C:H film was 2.5 μm thick); evidence of ferric element adhesion from the counterbody 1045 steel cylinder was found in the wear scar. This adhesion behavior was verified by photomicrograph and WDS Fe element mapping, as shown in Fig. 11(a) and (b), respectively. Additionally, adhesive and tribo-oxidative wear took place between the contact surfaces, inducing severe wear on the coating disk and counterbody 1045 steel.

***Hard Coatings and $Cr_{x\%}$-C:H Coatings Sliding against 1045 Steel Cylinder.*** Typically worn TiN or TiCN coating disks feature an adhesion reaction, as shown in Fig. 12(a). According to Fig. 12(a), there was a conglomeration adhesion to the worn coating surface. The same conglomerations were also back-transferred to the steel cylinder. The debris was created by tribochemical reaction between the wear pair. Its reddish brown color indicates that the major debris material is oxide $Fe_2O_3$,[32,33] accompanied by a few adhesion materials from the coating surface. A mixed process of adhesion and oxidation was the major wear process in this wear test. The typically worn surface of the

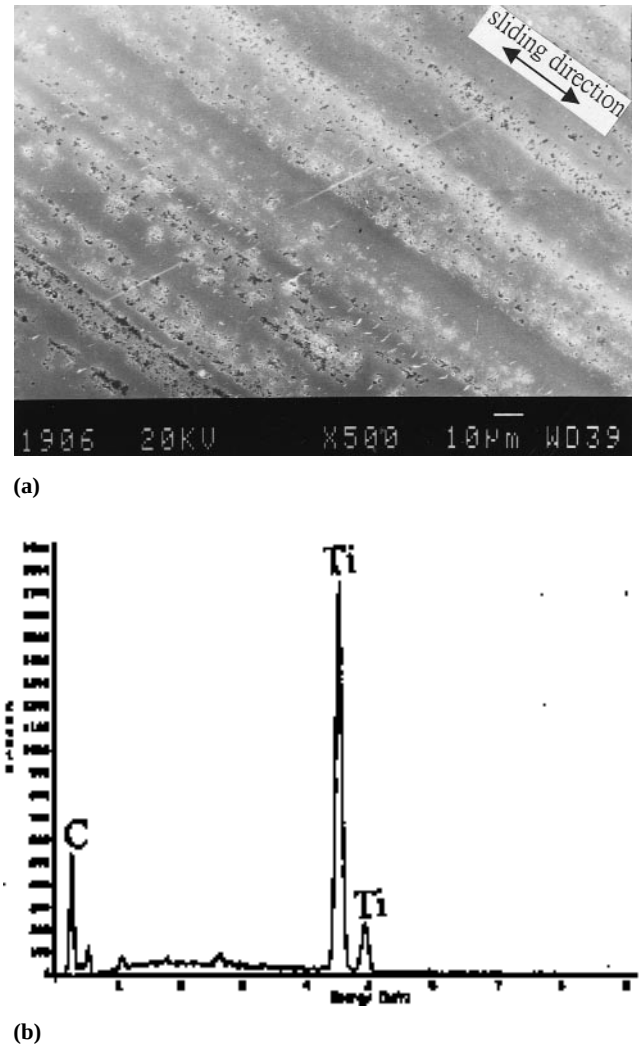


**Fig. 9** **(a)** Wear scar of the $Ti_{10\%}$-C:H coating disk against the 1045 steel cylinder under dry condition. **(b)** Corresponding EDS analysis of **(a)**

$Cr_{x\%}$-C:H coatings displays the similar worn feature of the TiN coating (Fig. 12(a)); this wear result also displays a mixed process of adhesive and oxidative wear. The typically worn feature of the CrN or CrCN coating displays a rubbed surface, as shown in Fig. 12(b); abrasive wear is the major wear process of this wear test. The adhesion material produced by tribochemical reaction did not influence measurement depth of the deepest wear scar on the coating disk; more detail can be found in Ref 34.

***Coatings Sliding against 7075T651 Al Cylinder.*** Two wear mechanisms of the $Ti_{x\%}$-C:H/7075T651Al or the $Cr_{x\%}$-C:H/ 7075T651Al wear pair took place during the wear test. First, a transfer layer was formed on the coating disk from 7075T651 Al when the wear tests were initially performed. The transfer layer was subsequently enlarged and then covered by the coating. Finally, a severe adhesion wear occurred on contact surfaces between coatings and 7075T651 Al wear pairs. The transferred Al layer on the coating disk not only negatively affect tribological properties (*e.g.*, noise, seizure, and high friction coefficients), but also induced severe adhesion damage on the coating

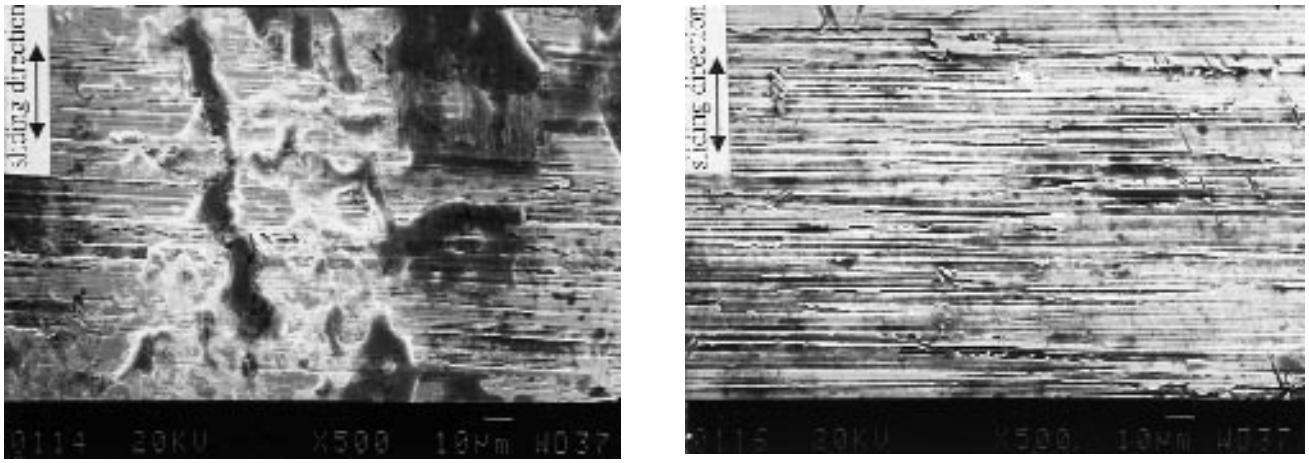


**(a)** **(b)**

**Fig. 10** The wear scar of the 1045 steel cylinder sliding against the $Ti_{10\%}$-C:H coating. **(a)** Transferred layer is formed on the 1045 steel cylinder. **(b)** The same wear scar of **(a)** after the transferred layer is removed

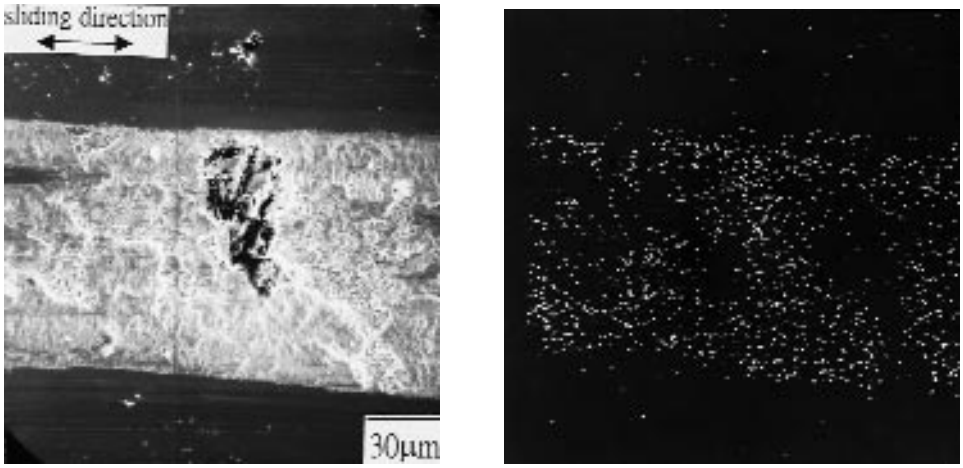


**(a)** **(b)**

**Fig. 11** **(a)** SEM photomicrograph of the wear scar on the $Ti_{30\%}$-C:H coating disk. **(b)** WDS Fe map of **(a)**, sliding against the 1045 steel cylinder under dry condition after testing for 50 s

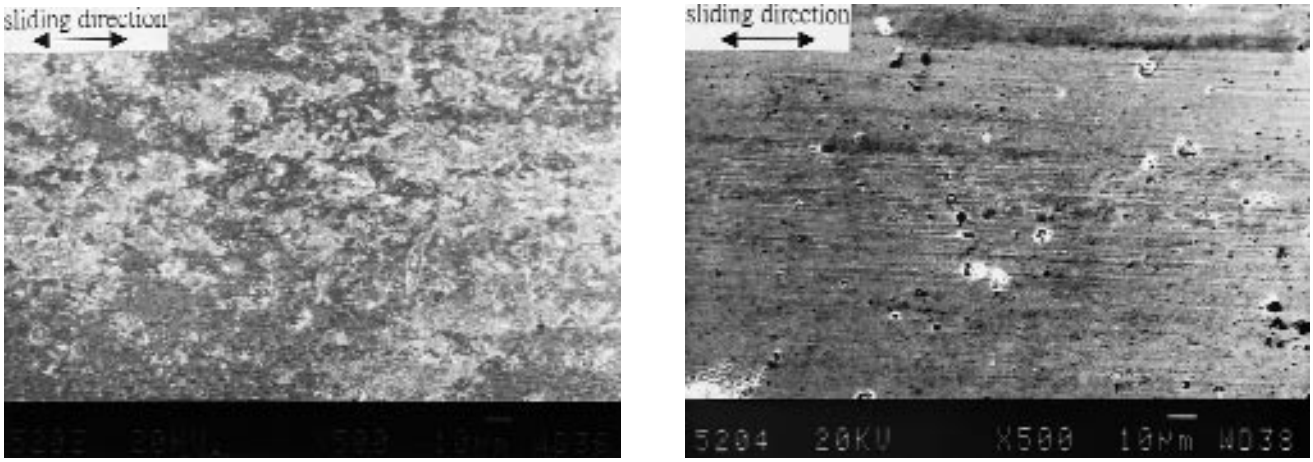


**(a)** **(b)**

**Fig. 12** **(a)** Typical worn surface of TiN, TiCN, and $Cr_{x\%}$C:H coatings. **(b)** Typical worn surface of CrN and CrCN coatings, sliding against the 1045 steel cylinder under dry condition

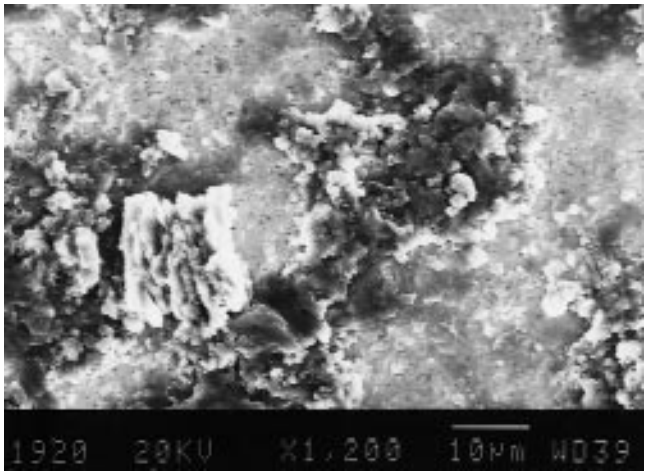


**Fig. 13** Typical worn surface of the $Ti_{x\%}$-C:H coating sliding against the 7075T651 A1 cylinder

surface. Figure 13 presents the typically worn surface of the coating disk ($Ti_{10\%}$-C:H coating with total 5.1 μm thickness) after testing for 24 min. Figure 13 demonstrates that the Al-transfer layer with lapped and conglomerate shapes has covered the worn coating disk, and some of the local coating layer has been pulled out, exposing the WC substrate (scar depth 5.1 μm). The hard coatings of TiN, TiCN, CrN, and CrCN were also damaged by a similar process under the tests, but they were less worn than the $Ti_{x\%}$-C:H and $Cr_{x\%}$-C:H coatings. The better resistance to wear of the hard coatings can be attributed to high microhardness and good adhesion between coating and substrate.

***Coating Sliding against Steel Ball.*** Figure 14(a) displays the typical wear scar on $Ti_{x\%}$-C:H coating disks with $x$ = 10 and 20% levels. The three gradation steps, denoted A, B, and C in Fig. 14a, correspond to the wear morphology of the substrate, medilayer, and $Ti_{x\%}$-C:H coatings, respectively. A detailed examination of the wear scar marks of the three gradation steps in Fig. 14(a), region A, confirms that the coating layer is completely worn through and the WC substrate is exposed. In addition, there is an Fe element adhesion from the steel ball on regions A and B. No Fe element was found on region C, implying that the transition of Fe element from the steel ball could have been averted if the $Ti_{x\%}$-C:H coatings had not worn through. Notably, the transition of the carbon-rich layer from the coating film did not appear in the wear scar on the steel ball because the wear debris was cleared out by the reciprocating action. Figure 14(b) reveals the black debris particles found around the circular edges of the typical wear scar on the 52100 steel ball. A detailed examination by EDS analysis indicates that this black material contained more carbon than the inner circular region. The softer coating and rich-carbon debris from the coating disk were eliminated from the contact surfaces, because the high-pressure reciprocating motion between the contact surfaces prevented a stable layer for establishing the lubricant. On the other hand, the $Ti_{30\%}$-C:H coating and all of the $Cr_{x\%}$-C:H coatings do not display the same gradation step wear morphology. According to the experimental results on the ball-on-disk, point-contact wear mode under dry conditions, the films of $Ti_{x\%}$-C:H or $Cr_{x\%}$-C:H coatings do not be-

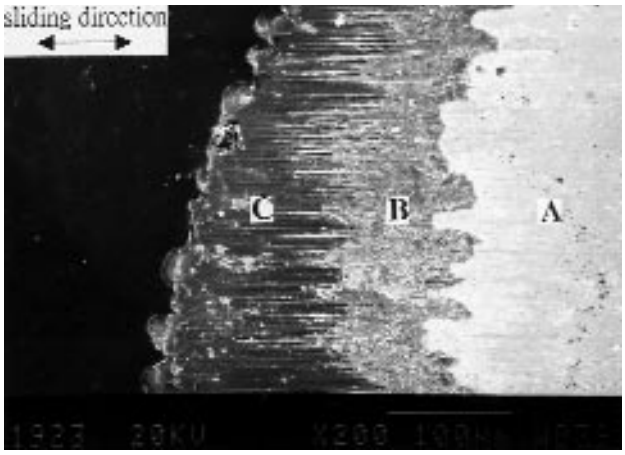


**(a)**

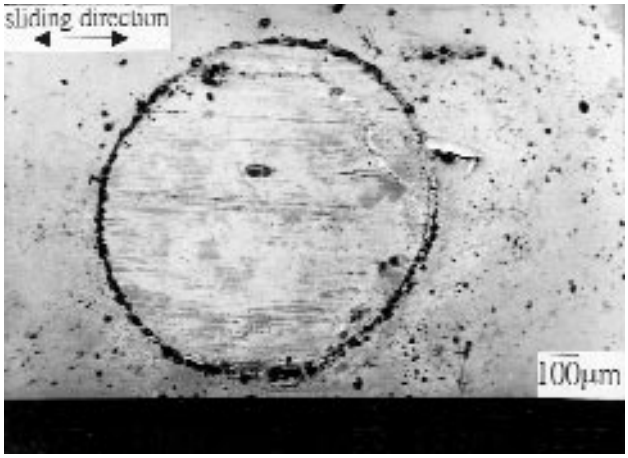


**(b)**

**Fig. 14** Typical wear surface of $Ti_{x\%}$-C:H/steel ball wear pairs. **(a)** $Ti_{x\%}$-C:H coating disk with $x$ = 10 or 20%. **(b)** Steel ball, wear test under dry condition

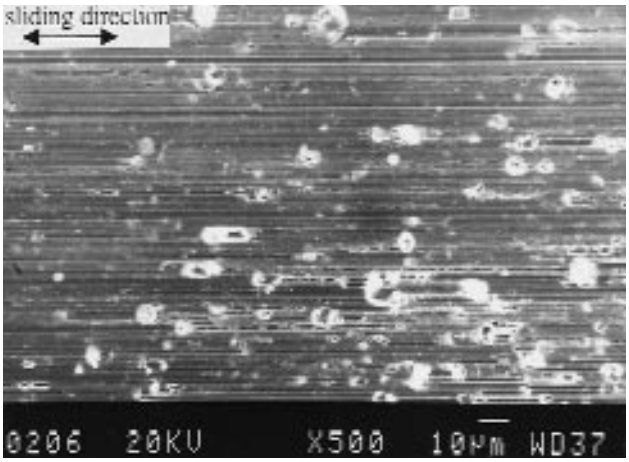


**Fig. 15** Typical wear surface of hard coatings (TiN, TiCN, CrN, and CrCN) sliding against the steel ball after testing for 24 min under dry condition

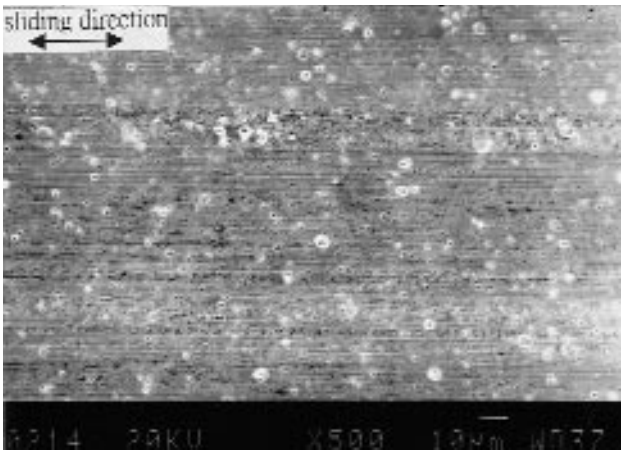


**Fig. 16** Typical wear surface of hard coatings (TiN, TiCN, CrN, and CrCN) sliding against the steel ball under HD-1 50 lubricated condition

have like solid lubricant under high pressure and reciprocating action. The worn surface of all hard coatings displays the mild rubbing traces typical of abrasive wear, as shown in Fig. 15.

### 4.2 Lubricated Conditions

Typically, a smooth curve represents the friction coefficient trace of hard coatings and Me-DLC coatings under the HD-150 and kerosene-lubricated conditions, for a coating disk sliding against a steel ball (ball-on-disk, point-contact wear mode). However, this does not apply to TiN and TiCN under kerosene-lubricated conditions. The typical worn surface of all hard coatings appears lightly rubbed and polished, as shown in Fig. 16. The rubbing behavior in this case is extremely mild. Therefore, the resulting smooth curve of friction coefficients and low wear can be attributed to the lubricant on cooling and lubrication. The $Cr_{30\%}$-C:H coating that possesses good wear resistance under lubricated conditions can be attributed to high microhardness of Me-DLC coatings and good adhesion strength. The $Ti_{30\%}$-C:H coating also has high microhardness, but it displays a poor wear resistance because of its very poor adhesion strength.

### 4.3 Special Wear Mechanism of TiN and TiCN under Kerosene-Lubricated Conditions

The typical friction trace reveals an initial high value under kerosene-lubricated condition for either TiN or TiCN coating disks against the steel ball (ball-on-disk, point-contact wear mode), as shown in Fig. 7(b). In tests conducted in lubricated sliding contact conditions, the material transfer and adhesion wear predominantly occurred while friction coefficients were between 0.6 and 0.9; this also induced fatigue fracture on the coating. Therefore, the initially high friction coefficient was due to the transferred layer formed on the coating disk during initial wear tests. A tribochemical reaction and the reciprocating rubbing action under high contact pressure induced severe wearing on the coating disks. A short test analyzed the tribological behavior between the contact surfaces of these wear pairs to discover why the coatings wore so severely during the wear tests. Figures 17(a) to (d) display the typical photomicrographs of the coating disk after testing for 3, 6, and 10 s and WDS Fe element mapping (corresponding to Fig. 17b), respectively. Initially, a layer was transferred from the steel ball to the wear scar on the coating disk, as shown in Fig. 17(a). Then, a local adhesion damaged and removed the TiN or TiCN coating layer, as shown in Fig. 17(b) and (d). Fatigue fracture from cracks in the transferred layer induced further catastrophic fracturing, and this rapidly enlarged the damage to the coating layer, as shown in Fig. 17(c). Finally, the WC substrate was exposed after testing for 31 s. The study compared tribological behavior of equally timed wear tests under kerosene and dry conditions. Figure 18 displays a typical wear scar of the TiN or TiCN coating; after testing for 3 s under dry condition, only a small amount of Fe material was transferred to the coating disk. The wear scars of Fig. 17(a) and 18 were qualitatively and quantitatively analyzed by EDS, as shown in Fig 19(a) and (b), respective to the wear scars in the figures. These analyses show that the amount of Fe element transferred to the wear scar under dry conditions (Fig. 19a) was about one-fifth of the amount transferred under kerosene conditions (Fig. 19b). This result suggests that, with a high level of friction, the kerosene enhanced the transfer of material from the steel ball to the TiN or TiCN coating, following the fatigue fracture on the transferred layer and coating, which induced the catastrophic coating fracture. In contrast, there was no layer transfer to the CrN and CrCN coatings and there was no adhesive wear under kerosene lubrication conditions. The typical worn surface comprised rubbing traces and the adhesion of a few Fe elements on coatings after testing for 24 min.

## 5. Conclusions

This study demonstrates that the Me-DLC coatings, $Ti_{x\%}$-C:H and $Cr_x$%-C:H, with different ratios *x*% of titanium or chromium target poisoning, and the hard coatings, TiN, TiCN, CrN, and CrCN, display significant differences in tribological properties and wear mechanisms. The following conclusions are based on the results in this study.

Under dry condition:

- The $Ti_{10\%}$-C:H coating is the optimum coating for the 1045 steel cylinder/coating disk, line-contact wear pairs. This coating displays low friction coefficients, low noise, and excellent wear resistance. Another characteristic of this coating is very small counterbody wear. Although CrN, CrCN, and $Cr_x$%-C:H coatings also display good wear resistance, they induce a high friction coefficient and more wear on the counterbody and produce loud noise during wear testing.
- Hard coatings (TiN, TiCN, CrN, and CrCN) display excellent wear resistance for the 7075T651 A1 cylinder/coating disk, line-contact wear pairs. However, severe adhesion damage pulls out the coating on Me-DLC ($Ti_{x\%}$-C:H and $Cr_{x\%}$-C:H) coating disks.
- Hard coatings (TiN, TiCN, CrN, and CrCN) display excellent wear resistance for steel ball/coating disk, point-contact

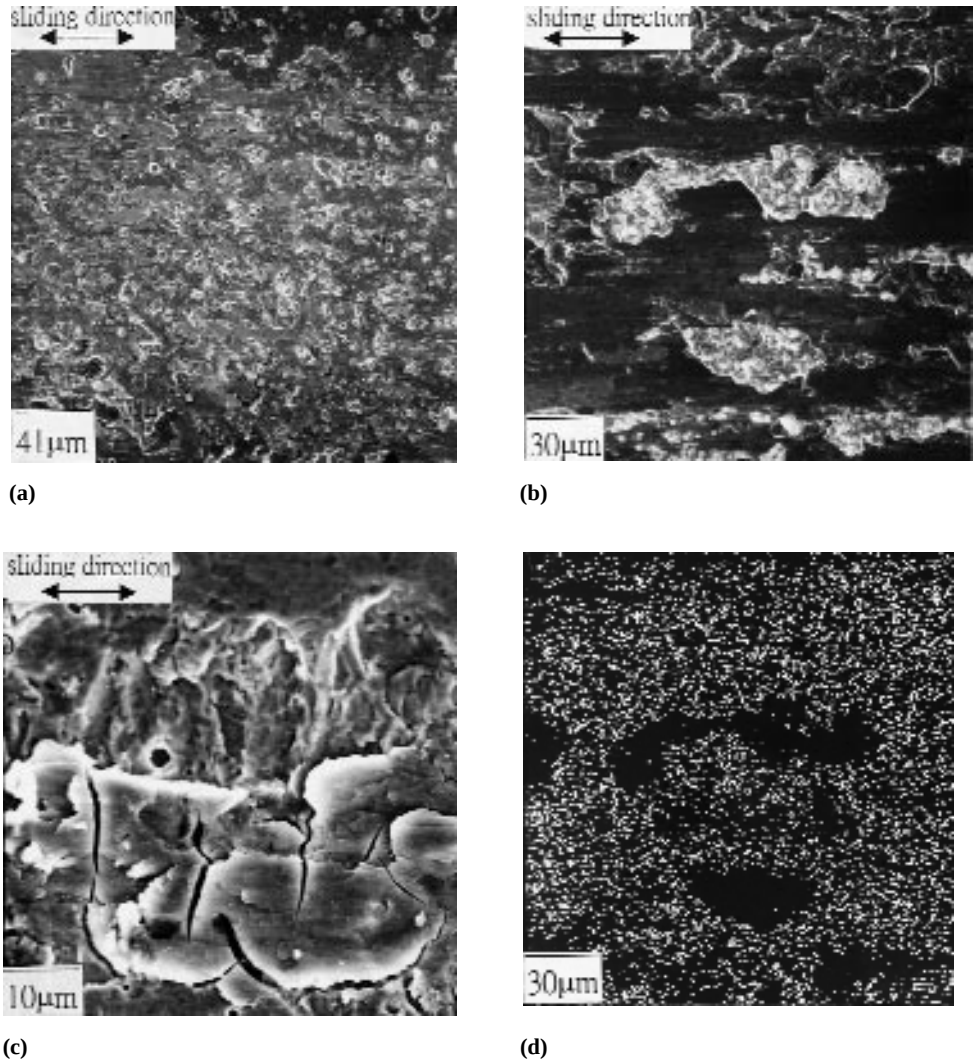


**Fig. 17** **(a** to **d)** The typical SEM micrographs of the coating disk after testing for 3, 6, and 10 s and WDS Fe element mapping (corresponding to b), respectively, for steel ball sliding against TiN or TiCN coating under kerosene-lubricated condition

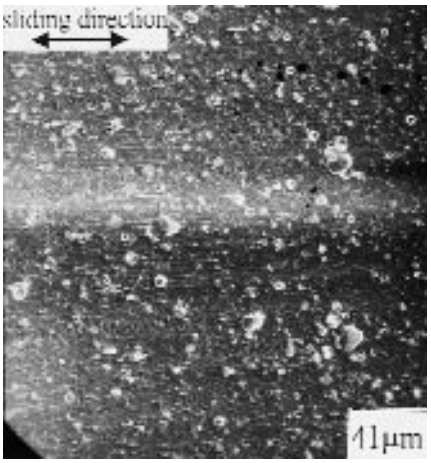


**Fig. 18** Typical wear scar of TiN or TiCN sliding against the steel ball after testing for 3 s under dry condition

wear pairs. In contrast, $Ti_{x\%}$-C:H and $Cr_{x\%}$-C:H coatings demonstrate unstable wear resistance under dry conditions because high contact pressure induces severe wear.

Under lubricated conditions:

- CrN, CrCN, and $Cr_{30\%}$-C:H coatings can be lubricated satisfactorily with excellent tribological behavior, such as extremely mild wear and low friction coefficients under HD-150 and kerosene-lubricated conditions. TiN and TiCN coatings also display excellent tribological behavior under the HD-150 lubricated condition. For $Ti_{x\%}$-C:H coatings, the lubricants (HD-150 and kerosene) do not provide effective protection on contact surfaces under high contact stress.
- There is a tribochemical reaction in tested steel ball/TiN and TiCN coating wear pairs under the kerosene-lubricated condition. Material transfers easily from the steel ball and forms on the TiN and TiCN coatings. Then, adhesive wear on the coating, along with fatigue damage from the transferred

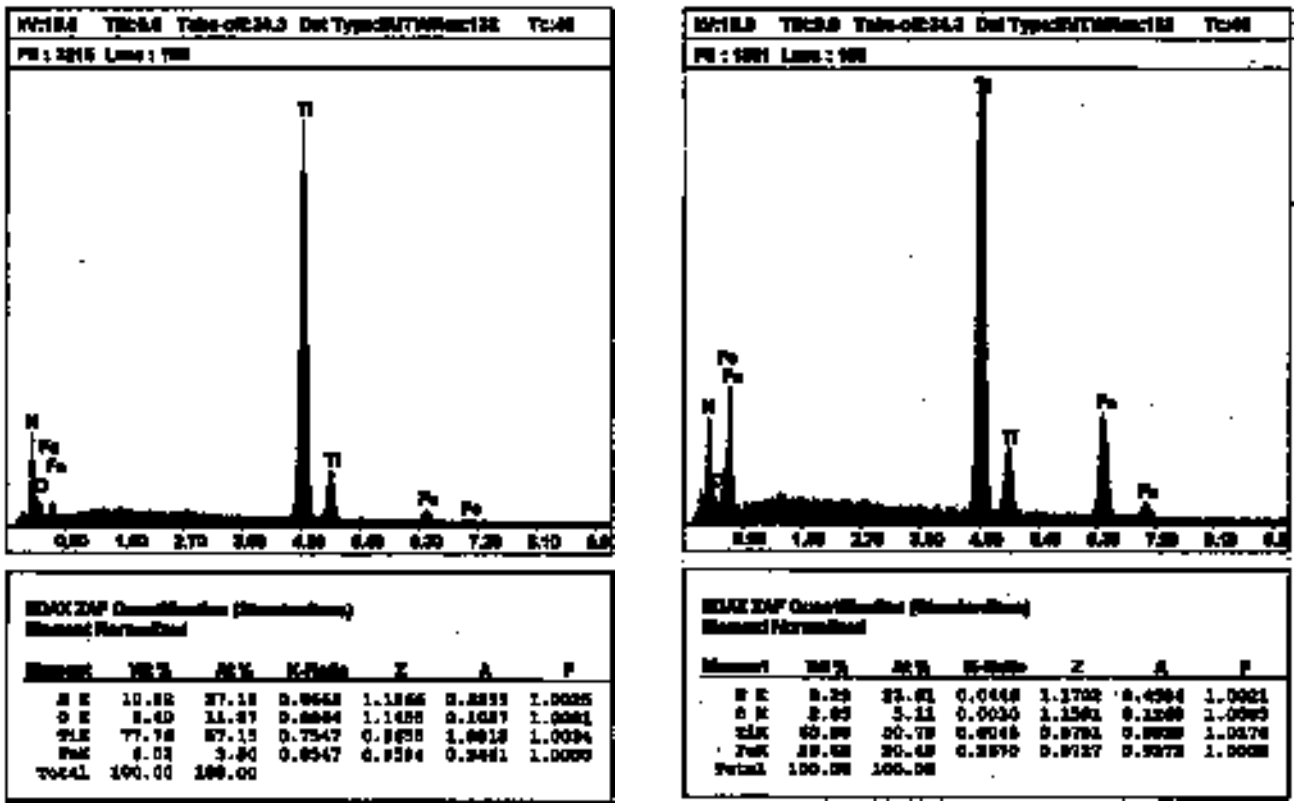

**(a)** **(b)**

**Fig. 19** EDS analysis of the coating wear scar of **(a)** Fig. 19 and **(b)** Fig. 17**(a)** corresponding to dry and kerosene conditions after testing for 3 s, respectively

layer into the coating layer, induces catastrophic fracturing on the TiN and TiCN coatings.

## Acknowledgments

The authors would like to thank the National Science Council of the Republic of China for financially supporting this research under Contract No. NSC 87-2212-E006-046 and the Cho Chang Tsung Foundation of Education for its financial support. Grateful thanks are especially dedicated to Mr. C. T. Wu for deposition.

## References

1. W.D. Sproul: *Surface Coating Technol.*, 1987, vol. 33, pp. 133-39.
2. G.R. Fenske: *STLE Tribology Trans.*, 1989, vol. 32, pp. 339-45.
3. P. Hedenquist, M. Olsson, P. Wallén, A. Kassman, S. Hogmark, and S. Jacobson: *Surface Coating Technol.*, 1990, vol. 41, pp. 243-56.
4. R. Porat: *Surface Eng.*, 1992, vol. 8 (4), pp. 292-94.
5. P.A. Dearnley, R.F. Fowle, N.M. Corbett, and D. Doyle: *Surface Eng.*, 1993, vol. 9 (4), pp. 312-18.
6. E. Bergmann, H. Kaufmann, R. Schmid, and J. Vogel: *Surface Coating Technol.*, 1990, vol. 42-43, pp. 237-51.
7. B. Navinsek: *Material and Manufacturing Processes*, 1992, vol. 7 (3), pp. 363-82.
8. S.K. Ghosh, and M.S. Koher: *Surface Coating Technol.*, 1992, vols. 54-55, pp. 466-69.
9. A. Wilson, A. Matthews, J. Housden, R. Turner, and B. Garside: *Surface Coating Technol.*, 1993, vol. 62, pp. 600-07.
10. A. Aubert, R. Gillet, A. Gaucher, and J.P. Terrat: *Thin Solid Film*, 1983, vol. 108, pp. 165-72.
11. Y. Chiba, T. Omura, and H. Ichimura: *J. Mater. Res.*, 1993, vol. 8 (5), pp. 1109-15.
12. H. Schulz, and E. Bergmann: *Surface Coating Technol.*, 1991, vol. 50, pp. 53-56.
13. S.H. Yao, and Y.L. Su: *Wear*, 1997, vol. 212, pp. 85-94.
14. A. Erdemir, M. Switala, R. Wei, and P. Wilbur: *Surface Coating Technol.*, 1991, vol. 50, pp. 17-23.
15. D. Klafke, R. Wasche, and H. Czichos: *Wear*, 1992, vol. 153, pp. 149-62.
16. Y. Liu, A. Erdenir, and E.I. Meletis: *Surface Coating Technol.*, 1996, vol. 82, pp. 48-56.
17. H. Ronkainen, J. Likoen, J. Koskinen, and S. Varjus: *Surface Coating Technol.*, 1996, vol. 79, pp. 87-94.
18. A. Erdemir, C. Bindal, G. Fenske, and P. Wilbur: *Tribolog. Trans.*, 1996, vol. 39, pp. 735-44.
19. A. Grill, B.S. Meyerson, and V.V. Patel: *IBM J. Res. Development*, 1990, vol. 34 (6), pp. 849-57.
20. A.G. Khurshudov, M. Olsson, and K. Kato: *Wear*, 1997, vol. 205, pp. 101-11.
21. D.P. Monaghan, D.G. Teer, P.A. Laing, I. Efeoglu, and R.D. Arnell: *Surface Coating Technol.*, 1993, vol. 60, pp. 525-30.
22. A.A. Voevodin, S.D. Walck, and J.S. Zabinski: *Wear*, 1997, vol. 203-204, pp. 516-27.
23. Stephen J. Harris, Anita M. Weiner, and Wen-Jin Meng: *Wear*, 1997, vol. 211, pp. 208-17.

24. Jianguo Deng, and Manuel Branu: *Diamond Related Mater.*, 1995, vol. 4, pp. 936-43.
25. D.P. Monaghan, D.G. Teer, and P.A. Logan: *Surface Coating Technol.*, 1993, vol. 60, pp. 525-30.
26. M. Wang, K. Schmidt, K. Reichelt, H. Dimigen, and H. Hubsch: *J. Mater. Res.*, 1992, vol. 7, pp. 667-75.
27. K. Bewilogua, and H. Dimigen: *Surface Coating Technol.*, 1993, vol. 61, pp. 144-50.
28. M.D. Bentzon, K. Mogensen, J.B. Hansen, C. Traeholt, P. Holiday, and S. S. Eskildsen: *Surface Coating Technol.*, 1994, vols. 68-69, pp. 651-55.
29. J. Koskinen, H. Ronkainen, J.P. Hirvonen, R. Lappalainen, and K.A. Pischow: *Diamond Related Mater.*, 1995, vol. 4, pp. 843-47.
30. S. Anders, A. Anders, J.W. Ager III, Z. Wang, G.M. Pharr, T.Y. Tsui, I.G. Brown, and C.S. Bhatia: *Mater. Res. Soc. Symp. Proc.*, 1995, vol. 383, pp. 453-58.
31. R.M. German: *Powder Metallurgy Sci.*, MPIF, Princeton, NJ, 1994, pp. 241-96.
32. T.F.J. Quinn: *Wear*, 1971, vol. 18, pp. 413-19.
33. T.F.J. Quinn: *Tribology Series 7*, Elsevier, Amsterdam, 1982, p. 579.
34. Y.L. Su, and W.H. Kao: *J. Mater. Eng. Performance*, 1998, vol. 7 (5), pp. 601-12.